Multiple-Model Estimation-based Prognostics for Rotating Machinery

Junyu Qi [1,2], Alexandre Mauricio [1,2], and Konstantinos Gryllias [1,2]

[1]*KU Leuven, Department of Mechanical Engineering*

[2]*Dynamics of Mechanical and Mechatronic Systems, Flanders Make*

Celestijnenlaan 300 B, B-3001, Heverlee, Belgium

junyu.qi@kuleuven.be
alex.ricardomauricio@kuleuven.be
konstantinos.gryllias@kuleuven.be

ABSTRACT

Data-driven based prognostics approaches are currently attracting unprecedented attention. Targeting towards more flexibility, statistical model based prognostics, which present more transparency and usually incorporate statistical models with stochastic filtering, are studied in this paper. Traditionally, versions of Kalman filters and Particle filters are combined with a single statistical model. However, the service life of a bearing undergoes several health stages, such as a normal stage, a slight degradation stage, and a severe degradation stage. Thus, a single model cannot represent well the full degradation process of a bearing. As such, the concept of Multi-Model Estimation (MME) has been introduced in the field of Condition Monitoring (CM) of rotating machinery. Initially the Switching Kalman Filter (SKF) has been proposed, combining three linear statistical models, based on the Classic Kalman filter (CKF), which on the other hand might be insufficient for nonlinearity estimations. In this paper, in order to overcome the drawbacks of the CKF, we extend the MME from the CKF to nonlinear system estimation techniques, such as the Extended Kalman Filter, the Unscented Kalman Filter and the Particle Filter. Additionally, in the proposed multi-model methodology, twelve statistical models are studied and used for automatic model switch. The methodology is tested and evaluated on fifteen experimental datasets and it can be concluded that the extended MME outperforms the classic switching Kalman Filter.

1. INTRODUCTION

Condition Monitoring (CM) attracts significant attention due to high industrial interest and economic potentials. Generally, CM includes three stages: fault detection, fault diagnosis, and fault prognosis. Fault detection and diagnosis provide respectively the existence and the root cause of machine defects. In view of a complete optimized maintenance strategy, it is important to monitor the machine status and estimate the Remaining Useful Life (RUL) in order to avoid sudden breakdowns and accidents.

Typically, prognostics literature can be categorized in three main methodology groups: the physics-based, the data-driven and the hybrid methods (Meng and Li 2019). Physics model-based approaches describe the parts' or the machine's degradation by explicit equations or Finite Element Models (FEM). However, these models are usually associated with numerous parameters, e.g., the material, the geometry, the speed, the load, etc. In contrast to the physics-models where a precise model is needed, data-driven models do not need detailed physical knowledge and accurate degradation evolution. On the contrary, data-driven methods are more flexible and their performance rely more on the quality of the collected data. In the state of the art, data-driven approaches are divided into the statistical model-based ones and the machine learning ones. Machine Learning (ML) is capable in general to learn the hidden information based on huge amount of data. It's possible to predict the RUL without the need of accurate mathematical models and signal processing techniques. However, the structure of neural networks seems like a black-box and the output is still hard to be interpreted in a physical sense.

Considering the flexibility and the cost of model construction, statistical model based approaches can be preferred. A data-driven methodology relying on the Extended Kalman Filter (EKF) and monitoring indicators (e.g. variance and Choi-Williams transform) has been proposed and evaluated on an experimental degradation dataset (Singleton, Strangas, and Aviyente 2015). Moreover the Unscented Kalman Filter (UKF) has been combined with self-organizing maps for bearing prognostics and has performed better than the EKF on an experimental dataset (Jin et al. 2019). Furthermore a Kalman smoother has been applied on a selected Health Indicator (HI) for prognostics of a high-speed shaft bearing of a wind turbine (Saidi et al. 2018). As explained above, the machinery's Health Status (HS) might go through several stages, e.g., the normal condition (healthy), the slightly degraded condition (pitting), and the extended damage (spall). Thus, Multi-Model Estimation (MME) has been proposed to overcome the deficiency of the classic stochastic filtering, which tracks the extracted HI using a single model. A Switching Kalman filter (SKF) (Lim and Mba 2015) estimated a bearing's RUL by three constant state space models to represent: a constant trend, a linear trend and a polynomial trend. At different HS (healthy condition, gradual wear, and accelerated wear), the corresponding model is switched. However, the classic SKF utilizes three linear models to track the degradation stages and as a result it can easily fail to work in the case of complex and higher nonlinearities. Thus, a multi-mode estimation (Wang, Yan, and Gao 2018) has been also derived for RUL prediction using a linear model and a nonlinear model.

In this paper, a MME based prognostics method, combining different prognostic indicators, estimators and statistical models, is proposed. The contribution of this paper consists mainly of the following two aspects:

1) Apart from the widely used in the state of the art exponential models, polynomial models are introduced for bearings' RUL estimation. In particular, the mixture of exponential and polynomial models are proposed to remedy the weakness of a single exponential model or a single polynomial model.

2) In order to overcome the weakness of the classic SKF in the case of high nonlinearities, the Multi-Model Estimation (MME) is extended to advanced versions of Kalman Filters and Particle Filters, : EKF, UKF, Ensemble Kalman Filter (EnKF), PF, Auxiliary PF (APF) and Rao-Blackwellized PF (RBPF), combining a library of nonlinear statistical models.

The rest of the paper is organized as follows: in Section 2, the applied HIs, the theory of estimators and the proposed MME are introduced. Then, an experimental dataset is detailed in Section 3. In Section 4, the proposed methodology is applied and the RUL prediction results are subsequently discussed. Finally, the conclusions of the paper are presented in Section 5.

2. THEORY

In this section, the applied HIs are firstly reviewed. Then, advanced versions of Kalman Filters and Particle Filter are briefly presented. Furthermore, the classic SKF and the proposed MME are explained.
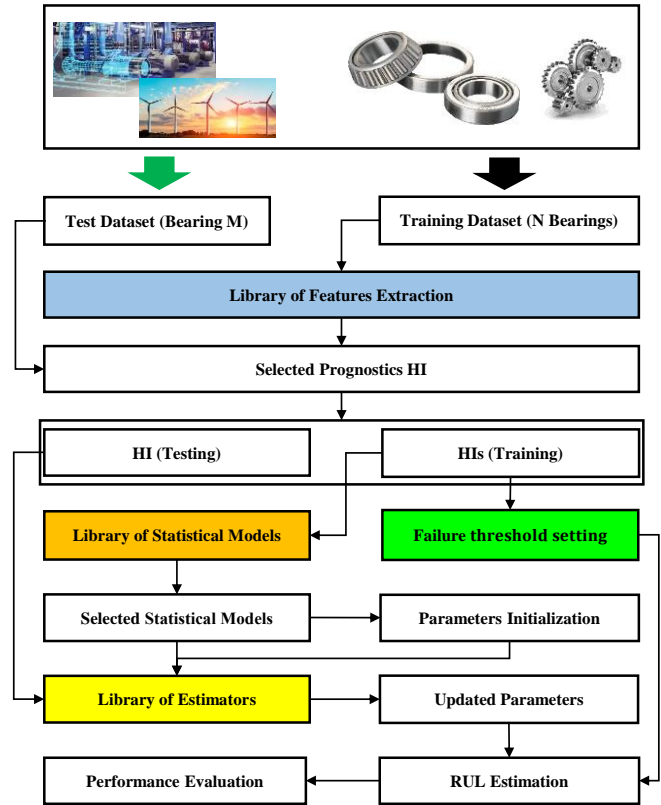
Figure 1. Flowchart of statistical model based prognostics

Before detailing each individual step, the methodology of statistical model based prognostics is presented in Figure 1. The flowchart mainly involves four key steps: (1) HI extraction, (2) Statistical model, (3) Estimator, and (4) Failure Threshold. Firstly, data is measured on the monitored machine (e.g. a wind turbine, a motor, etc.), which runs under an operating condition. The acquired historical datasets (e.g. from N bearings) are used as training data and a number of HIs can be calculated. In order to improve the RUL prediction performance, a high quality HI is selected, based on the training data, considering their trendability and prognosability (Jamie, Coble, Hines 2009). Then, the statistical model and the failure threshold can be determined. When new data is captured from the on-line operating machinery, the selected HI will be extracted.Moreover, the HI of the testing data is loaded to the estimator and the statistical model, e.g. the corresponding model parameters, can be online (almost real-time) updated. Finally, by the extrapolation to the predefined failure threshold, the estimated RUL is calculated.

2.1. Prognostics indicator extraction

As shown in Figure 1, HI extraction is the first step after the data acquisition. Thus, it plays a vital role for the future RUL estimation. To guarantee the quality of the prognostics HI, a large set of HIs is analyzed and their performance is compared based on the criteria of trendability and prognosability.

2.1.1. Applied HIs

In order to capture different types of defects (e.g. localized faults presenting high impulsiveness, distributed faults presenting low impulsiveness etc.), an extended number of HIs are extracted in the aspect of entropy and sparsity. In the end, they are compared with some classic statistics indicators, e.g. RMS, Kurtosis (K), Peak to Peak (P2P) and Spectral Kurtosis (SK). Due to the text limitation, the applied indicators will be very briefly introduced and their details can be found in the given references.

1) Spectral Entropy

Spectral or Shannon Entropy ($SpecE$) measures the disorder of the spectrum of a signal (Pan, Chen, and Li 2009).

2) Spectral Negentropy

Spectral Negentropy ($NegE$), equal to the reverse of Entropy, measures the order of data. It deals not only with impulsive events but also with repetitive transients. The NegE of the Squared Envelope (SE) I_{SE}, the Squared Envelope Spectrum (SES) I_{SES} and their average form $I_{1/2}$, are used in Infogram (Antoni 2016) .

3) Spectral Flatness

Spectral Flatness (F_{spec}), also termed as Wiener entropy, has been widely applied in the audio processing (Gray and Markel 1974). F_{spec} is a measurement of likeliness between a signal and white noise. Following F_{spec}, Flatness is extended on the SE (F_{SE}) and the SES (F_{SES}). In the case of a signal having high impulsiveness, Flatness presents a low value.

4) Spectral Sparsity

Sparsity is a measure of few non-zero elements of a raw or matrix. It can be quantifies by different indicators: $L2/L1$, $L1/L0$, Gini index and Quasi-Arithmetic Means (QAM) (Hou et al. 2021). $L2/L1$ is mathematically equivalent with SK. $L1/L0$ and Gini index ($Gini$) are less sensitive to outliers. QAM exhibits an earlier detection and a better degradation tendency than other sparsity indicators (Hou et al. 2021). All sparsity indicators are calculated on the SE and the SES. In Table 1, they are given as: X_{SES} and X_{SES}, where X is the corresponding sparsity indicator. Details of 11 QAM (QAM1, QAM2, …, QAM11) indicators can be found in (Hou et al. 2021).

Table 1. Library of applied HIs.

		Applied HIs
Entropy	$SpecE$	1) $SpecE$
	$NegE$	2) I_{SE} 3) I_{SES} 4) $I_{1/2}$
	Flatness	5) F_{Spec} 6) F_{SE} 7) F_{SES}
Sparsity	$L2/L1$	8) $L2/L1_{SE}$ 9) $L2/L1_{SES}$
	$L1/L0$	10) $L1/L0_{SE}$ 11) $L2/L1_{SES}$
	$Gini$	12) $Gini_{SE}$ 13) $Gini_{SES}$
	QAM	14) $QAM1_{SE}$ 15) $QAM1_{SES}$
		16) $QAM2_{SE}$ 17) $QAM2_{SES}$
		18) $QAM3_{SE}$ 19) $QAM3_{SES}$
		20) $QAM4_{SE}$ 21) $QAM4_{SES}$
		22) $QAM5_{SE}$ 23) $QAM5_{SES}$
		24) $QAM6_{SE}$ 25) $QAM6_{SES}$
		26) $QAM7_{SE}$ 27) $QAM7_{SES}$
		28) $QAM8_{SE}$ 29) $QAM8_{SES}$
		30) $QAM9_{SE}$ 31) $QAM9_{SES}$
		32) $QAM10_{SE}$ 33) $QAM10_{SES}$
		34) $QAM11_{SE}$ 35) $QAM11_{SES}$

2.1.2. Prognostics HI selection

To select a high quality prognostics HI, the 35 indicators presented in Table 1 are combined with a 1/3-binary tree, which is regularly used in diagnostic tools such as Fast Kurtogram, Infogram and Sparsogram. Vibration signals are firstly decomposed into many sub-signals of different frequency bands. Then, Kurtosis, Negentropy and Sparsity of these sub-signals are calculated. Thus an extended library of HIs is extracted, based on the 35 indicators calculated on all decomposed sub-signals. Then, data from N training bearings are analyzed and N curves are calculated, in each specific frequency band for each HI of Table 1. It is important to select the HI from a specific frequency band which presents the highest trendability (TRD) and prognosability (PRG) (Jamie, Coble, Hines 2009). TRD reflects how early and well the degradation tendency is. PRG measures the variance of the failure points of HIs, which are linked with the failure threshold setting. Good TRD and PRG will finally improve the performance of the RUL prediction. Therefore, a score of the average TRD and PRG is set to select the HI.

2.2. Versions of estimators

Kalman Filters and Particle Filter belong to the typical stochastic filtering approaches. Gaussian noise is assumed in the process and in the measurements. In a prediction step, the priori estimation and the uncertainty are produced. When a

new measurement becomes available, the posteriori estimation is updated.

1) Classic Kalman Filter

The Classic Kalman Filter (CKF) has been proposed for a linear system, which is perturbed by errors that coincide with the Gaussian noise (process noise and measurement noise).

2) Extended Kalman Filter

The Extended Kalman Filter (EKF) has been proposed for a system with low nonlinearities. After linearizing the state transition function and the observation function, a Jacobian matrix is calculated at each time step. In this way, the estimation of the nonlinear system is changed to a linear system.

3) Unscented Kalman Filter

In order to remedy the problem of EKF in the case of high nonlinearities, the Unscented Kalman Filter (UKF) uses a number of samples and the corresponding weights to approximate the state and the covariance.

4) Ensemble Kalman Filter

The Ensemble Kalman Filter (EnKF) (Roth et al. 2017) is a Monte Carlo approximation of the Kalman Filter. Using a set of samples (or particles), the state covariance in the Kalman gain matrix can be replaced by the sample covariance. Compared to the Particle Filter, the EnKF is more efficient by avoiding the resampling step.

5) Particle Filter

The Particle Filter (PF) estimates the state by many particles. After the propagation of these particles, the Probability Density Function is updated by a resampling strategy. Particles with low likelihood are rejected and only high weight particles are kept.

6) Auxiliary Particle Filter

The Auxiliary Particle Filter (APF) (Arulampalam et al. 2002) is an improved PF dealing with the deficiencies of classic PF, such as the tailed observation density. Instead of blindly draw particles from the prior density, APF favors particles from a joint distribution, which combines not only the prior density, but also the likelihood by incorporating the measurement in the update step.

7) Rao-Blackwellized Particle Filter

Rao-Blackwellized PF (RBPF) (Mustière, Bolić, and Bouchard 2006) marginalizes the probability distribution of the state rather than the direct sampling from the multivariable probability distribution. In particular, it can be more efficient for higher dimension of the states, which requires normally more particles using generic PF.

2.3. Proposed Multiple Model Estimation (MME)

Traditionally, the Switching Kalman Filter (SKF) (Lim and Mba 2015) determines the model states with several dynamical models in parallel. The states and the probability of each model are computed using the CKF at each time step. Then, the estimated states are a combination of the contribution of n models. In the referred source, three constant state space models (zero, 1st and 2nd order Kalman filter) are used to represent respectively the stationary trend, the linear trend and the polynomial trend.

Although the SKF has been proposed to overcome the disadvantages of tradition single model estimation, it estimates the models' states using the CKF, which might fail to track the severe damage by the constant state transition matrix. Therefore, instead of the CKF, it is worthy to investigate the estimation with other versions of KF and PF. In addition, three constant state space models of the SKF have the same dimension and physical meaning so that the estimated states of one model can interact with another model. From this point of view, many nonlinear models of the state of the art cannot be jointly integrated. To tackle this problem, the proposed MME follows the strategy of a Multi-Mode Estimation (Wang et al. 2018), which merged two self-selected models: a linear model and a nonlinear model, to the PF. In the end, the model is switched by comparing the likelihood of different models.
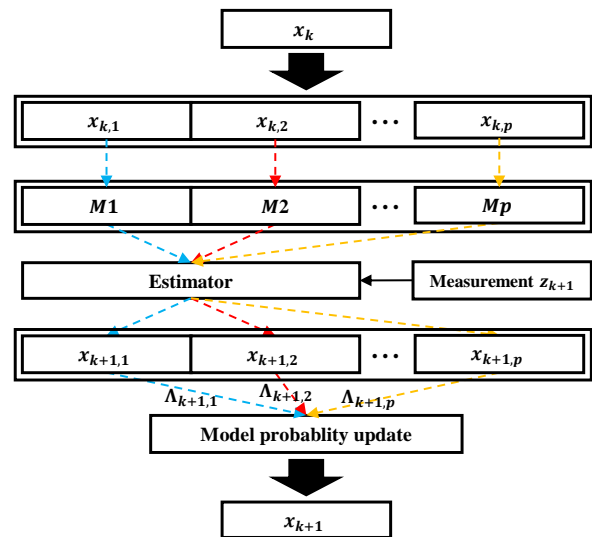
Figure 2. Principle of extended MME

In Figure 2, the principle of the extended MME is illustrated. At step k, the state x_k, i.e., $x_{k,1}, x_{k,2}, \ldots, x_{k,p}$, is prepared for a library of statistical models: $M1$, $M2$, $\ldots$, Mp. By incorporating the models with the versions of estimators, presented in the section 2.2, and the measurement z_{k+1}, the state at step $k+1$ is estimated for each model, that is, $x_{k+1,1}, x_{k+1,2}, \ldots, x_{k+1,p}$. Unlike the classic SKF, which restricts the three constant state space models, the proposed

strategy can integrate any number of statistical models together. The estimation of these models are computed in parallel. By comparing the likelihood between the estimation and the new measurement, the model with the highest likelihood will be automatically switched.

A library of statistical models (indexed in format of 'Mx', x=1,…, 12) in Table 2 are merged to the proposed MME strategy presented in Figure 2. In order to have a thorough study, these 12 statistical models cover not only the most frequently used exponential models ('Exp'), e.g. M3, M4 and M6, but also two Polynomial models ('Poly'). Additionally, to overcome the limitation of a single model, e.g. in the case of a HI with multiple characteristics or a set of HIs with different natures, the mixture types of exponential and polynomial models ('Exp'+'Poly') are proposed. The parameters a, b, c, d (with subscripts) stand for the model parameters, t is the time index.

Table 2. Library of statistical Models.

		Model equation
'Poly'	M1	$a \cdot t + b$
	M2	$a \cdot t^2 + b \cdot t + c$
'Exp'	M3	$a \cdot e^{b \cdot t}$
	M4	$a \cdot e^{b \cdot t + \vartheta - \sigma^2/2}$
	M5	$a \cdot e^{b \cdot t^2}$
	M6	$a \cdot e^{b \cdot t} + c \cdot e^{d \cdot t}$
'Poly' + 'Exp'	M7	$a_1 \cdot t + b_1 + a_2 \cdot e^{b_2 \cdot t}$
	M8	$a_1 \cdot t + b_1 + a_2 \cdot e^{b_2 \cdot t^2}$
	M9	$a_1 \cdot t + b_1 + a_2 \cdot e^{b_2 \cdot t} + c_2 \cdot e^{d_2 \cdot t}$
	M10	$a_1 \cdot t^2 + b_1 \cdot t + c_1 + a_2 \cdot e^{b_2 \cdot t}$
	M11	$a_1 \cdot t^2 + b_1 \cdot t + c_1 + a_2 \cdot e^{b_2 \cdot t^2}$
	M12	$a_1 \cdot t^2 + b_1 \cdot t + c_1 + a_2 \cdot e^{b_2 \cdot t} + c_2 \cdot e^{d_2 \cdot t}$

3. EXPERIMENTAL DATA

The experimental test rig (Wang et al. 2020) consists of an AC motor, a motor speed controller, support bearings, a test bearing and hydraulic loading. The tested bearings have an outer race diameter equal to 39.80 mm, an inner race diameter 29.30 mm and dynamic load rating 12.82 kN. Experimental datasets are captured in three operating conditions: C1 (2100 RPM, 12 kN), C2 (2250 RPM, 11 kN), C3 (2400 RPM, 10 kN). The horizontal and vertical vibration data are simultaneously acquired with a sampling frequency of 25.6 kHz. The measurements are recorded for 1.28 seconds with an interval of 1 minute. Finally, five degraded bearings have been recorded for each operating condition. These 15 bearings are indexed in format of 'BCI', B: bearing, C: condition, I: bearing index).
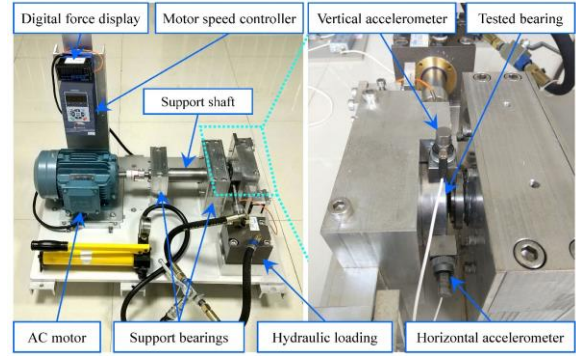
Figure 3. Experimental test rig.

4. RESULTS AND DISCUSSION

In this section, the extracted HIs and the RUL prediction results are presented.

4.1. Extracted prognostics health indicator

Sequences of five bearings are available in each operating condition. Data of the four bearings are iteratively chosen for training and data from the fifth one are used for testing. Then, based on the predefined score mentioned in Section 2.1.2, the prognostics HI is selected for each test bearing. The 35 HIs presented in Table 1 are firstly calculated using the experimental data. The extracted SK of the B11 is displayed in Figure 4 (a), where the B14 demonstrates an extreme increase at the end stage, while the B11, B12 and B13 show a worse (fluctuating and decreasing) tendency after the middle stage. However, by analyzing the Figure 4 (b) it can be concluded that the selected HI for the B11 shows an increasing trend almost since the beginning, and the 'thr' from the other four bearings nearly coincides with the end point of B11. In addition to the visual check, it can be seen in Table 3 that the score of the QAM is much higher than the four classic HIs: RMS, Kurtosis (K), Spectral Kurtosis (SK), and Peak to Peak (P2P). Regarding the other bearings, the selected HIs are vividly unveiled in Figure 5. QAM presents a better performance compared to the candidate HIs.
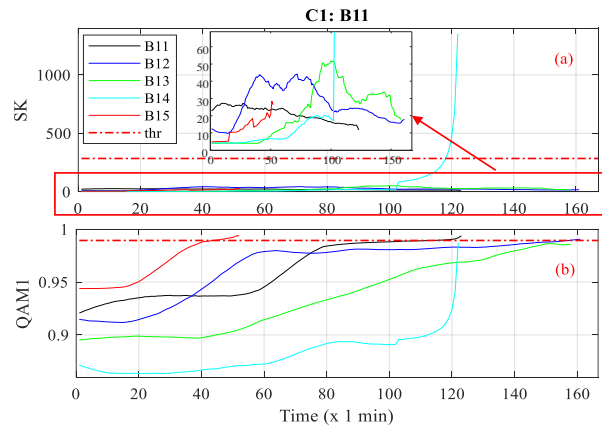
Figure 4. HIs of B11, (a) SK, (b) QAM1

Table 3. Library of statistical Models.

	RMS	K	P2P	SK	QAM
Score	0.675	0.319	0.755	0.324	0.937
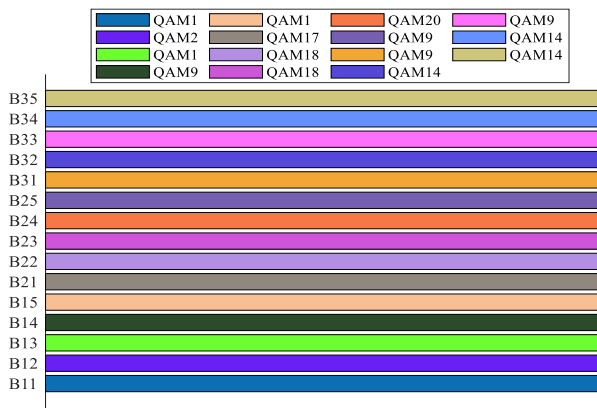
Figure 5. Selected features for the three conditions

4.2. RUL estimation results

Using the extracted HIs of the training datasets, the failure threshold is set equal to the averaged end point. After the preparation of the prognostics HI, the statistical models and the failure threshold, the model parameters can be continuously updated and the RUL is on-line calculated by the extrapolation to the threshold. Due to space limitation, only the B11 results are presented here. The RUL calculated by the classic SKF is firstly given. Then, the estimated results by all models listed in Table 2 and the estimators mentioned in Section 2.2 are presented. In the end, the comparison of the extended MME with the classic SKF and the comparison of the different models and the estimators are summarized.
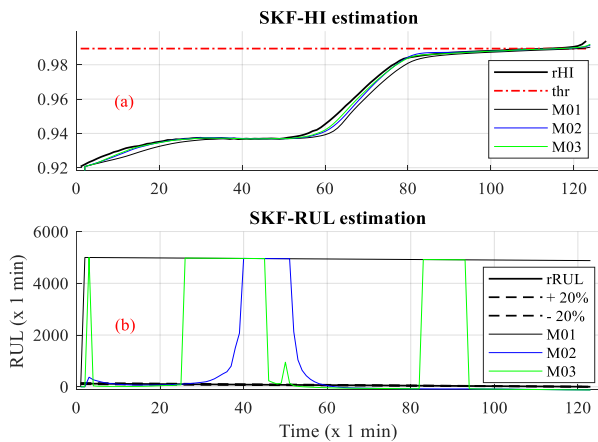
Figure 6. (a) HI estimation (b) RUL estimation of B11 by the classic SKF

In Figure 6, the estimated HI and the RUL estimated by the classic SKF are shown respectively in (a) and (b). The real HI exhibits a slight increase before 20 (x 1 min) but then is stabilized between 30 (x 1 min) and 60 (x 1 min). After that,

the HI increases steeply till around 80 (x 1 min). At the last stage, the real HI displays more or less a stable tendency. The HI estimations by three constant models: zero order ('M01'), 1st order ('M02') and 2nd order ('M03') follow a similar path. The probability of each model can be seen in Figure 7 (a). 'M01' has almost the highest probability before 60 (x 1 min), which means that the machine status for this period is recognized as healthy. From 60 (x 1 min) to around 80 (x 1 min), the 'M02', standing for the slight wear, is computed as the most probable model. After that, the 'M01' is switched again at the last stage. The switched model, corresponding to the model probability, is shown in Figure 7 (b). Based on i) the information of the estimated HI (Figure 6), ii) the RUL estimated by 'M01', 'M02' and 'M03' (Figure 6) and iii) the information of the most probable model (Figure 7 (b)), the switched HI and RUL are calculated and described in Figure 8 (a) and (b). The section of the estimated RUL by the 'M01' has a relative large error, as no trend can be extracted by a zero order model. Thus, the RUL estimation only converges closer at around 20 (x 1 min) and at the period of 60 (x 1 min) to 80 (x 1 min), when the 1st order model is switched.
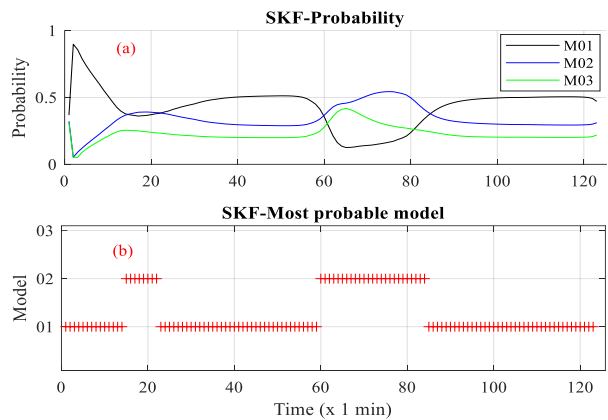
Figure 7. (a) Probability (b) Most probable model of three linear models by the classic SKF on B11
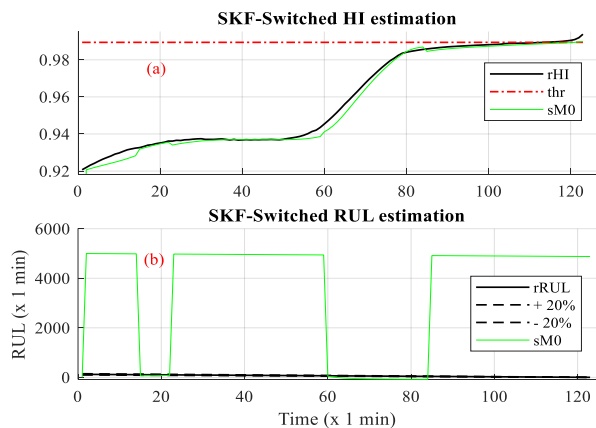
Figure 8. (a) Switched HI estimation (b) Switched RUL estimation of B11 by classic SKF
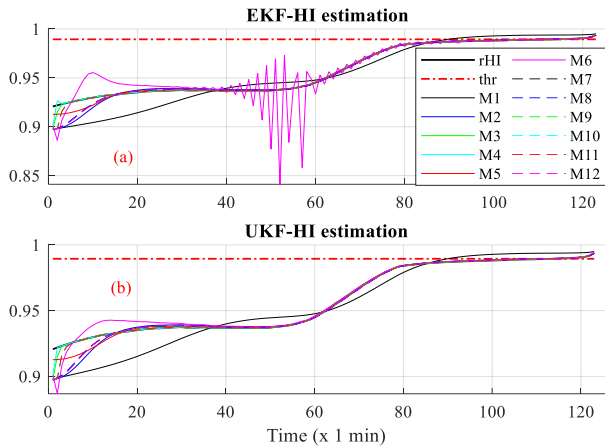
Figure 9. HI estimation of B11 by 12 models and (a) EKF (b) UKF

Before presenting the switching results based on the proposed methodology, the estimations by different models (in Table 2) are firstly compared. In Figure 9 (a), the real HI ('rHI') is estimated by the EKF and the 12 models ('M1', ..., 'M12') of Table 2. M1 follows the general trend of the real HI, while M6 estimates the curve with a large error before 20 (x 1 min) and then converges closer to 'rHI' at around 40 (x 1 min). After that, possibly due to the linearization of EKF, the estimation becomes diverse till 60 (x 1 min). Further, the other 10 models, including the proposed mixture types (M7, M8, ..., M12), track almost similarly close to 'rHI'. For the UKF with the same 12 models, 'M1' estimates the HI quite similar with the EKF. Regarding 'M4', the curve by the UKF has been significantly improved, especially with less fluctuations between 20 (x 1 min) and 80 (x 1 min). Thus, it is rather possible that the severe fluctuation in Figure 9 (a) arises from the linearization of the EKF.

Accordingly, the RUL estimation of the 12 models are compared for each estimator, which is exhibited in Figure 10, 11 and 12, respectively. For the estimated RULs in Figure 10 (a), the 'M6' with the EKF has serious fluctuations between 40 (x 1 min) and 50 (x 1 min), which coincides with the estimated HI in Figure 9 (a). After that, the estimated RUL cannot converge well to the real RUL. Another noticeable curve 'M4' indicates a prolonged RUL while time goes on. Besides, 'M3' estimates the RUL well before 40 (x 1 min), then starts to diverge far from the real RUL. Further, 'M5' performs good prediction before 90 (x 1 min), but overestimates the RUL at the last stage. Finally, it can be found that the proposed mixture models ('M7', 'M8', ..., 'M12') converges closer to the real RUL than the popular exponential models, a visual difference is obviously seen before 60 (x 1 min). For UKF estimation in Figure 10 (b), 'M4' and 'M6' discloses large estimation error, while 'M1' and 'M3' track almost along the real RUL. Compared to 'M2' and 'M5', estimations by mixture models (dash lines) approach closer to the real RUL. In Figure 11 (a), 'M3' and

'M9' combined with EnKF attain relative good RUL estimation. Like other estimators, 'M4' and 'M6' fail to extrapolate useful RULs for B11, while the mixture models gain superior performance than 'M1' and 'M5'. Regarding classic PF in Figure 11 (b), 'M3' and 'M5' have similar estimation with EnKF. The mixture models have better prediction than 'M2' and 'M5'. In Figure 12 (a), the estimated RUL by APF has similar performance with classic PF. 'M3' and 'M9' converge closer to real RUL compared to other models. Yet, the estimation by 'M4' is significantly improved compared to the classic PF, it converges to real RUL at the last stage. In Figure 14 (b), although 'M3' and 'M9' still win the best prediction in RBPF, the performance of other curves (e.g. 'M7' and 'M8') differs slightly from the classic PF and APF. The bump between 40 (x 1 min) and 60 (x 1min) is a bit higher than other versions of PF. Furthermore, 'M2' and 'M5' estimate more accurate than classic PF and APF.
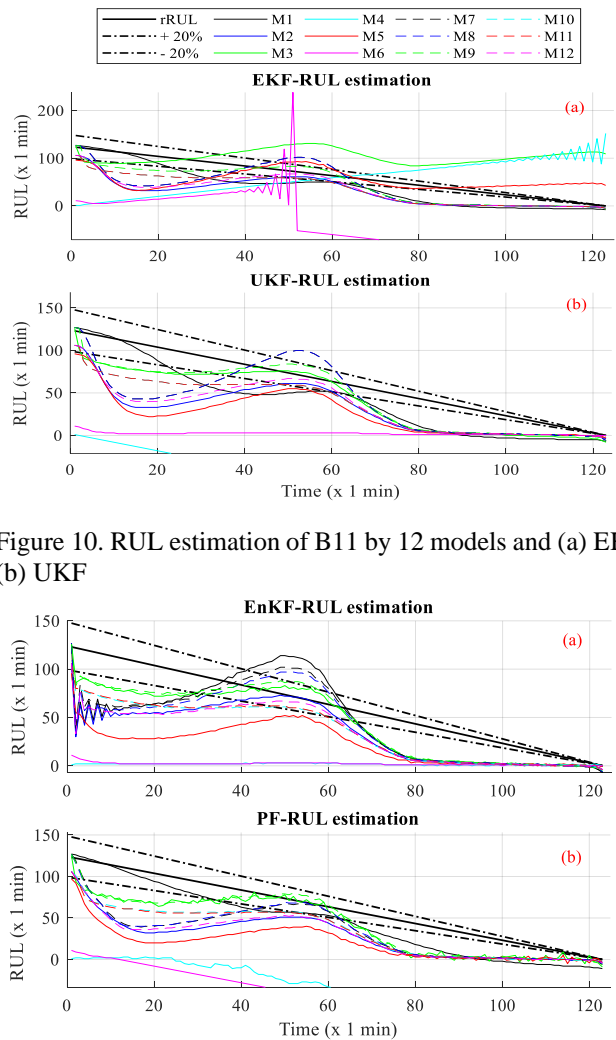
Figure 10. RUL estimation of B11 by 12 models and (a) EKF (b) UKF
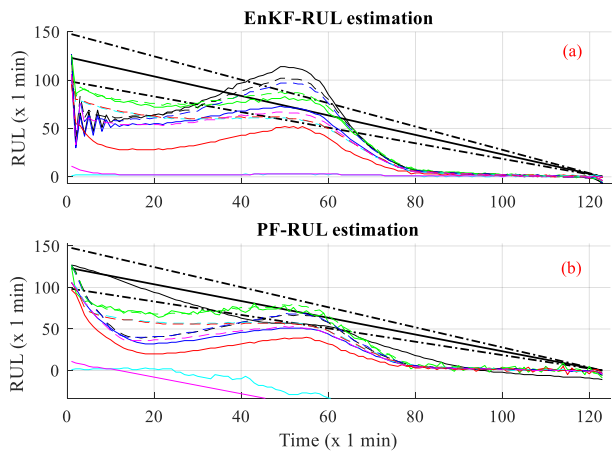
Figure 11. RUL estimation of B11 by 12 models and (a) EnKF (b) PF
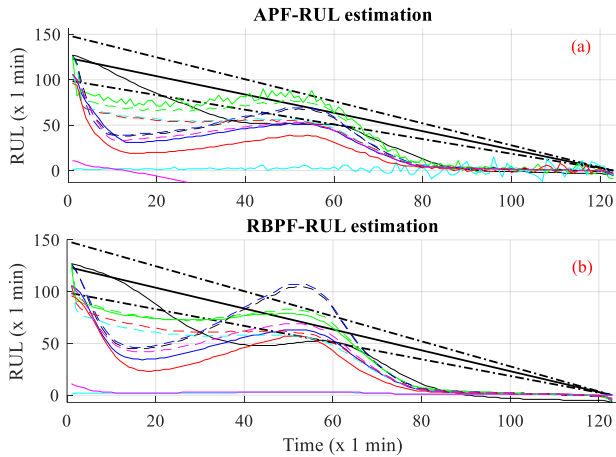
Figure 12. RUL estimation of B11 by 12 models and (a) APF (b) RBPF

As explained in Section 2.3, the model is continuously switched by comparing the maximal likelihood of 12 models. In Figure 13 (a) and (b), switching EKF and switching UKF has quite similar switched models. 'M12' and 'M5' switch frequently before 40 (x 1 min). Then, from 50 (x 1 min) till the end, 'M2' and 'M8' hold for a long period. Analyzing Figure 13 (c), (d) and (e), models are changed more frequently between 'M1' and 'M12', it is caused by the strategy of particles. A large amount of particles are randomly generated from a prior distribution, during the particles' propagation, the estimation of different models may have a higher or lower likelihood to the measurement. However, the enhanced PF, switching RBPF in Figure 13 (f) has less switching frequency than other versions of PF. The model is firstly switched to 'M9' and 'M11' before 20 (x 1 min), then use 'M4' to 50 (x 1 min). From around 70 (x 1 min) on, 'M5' is chosen till the end.
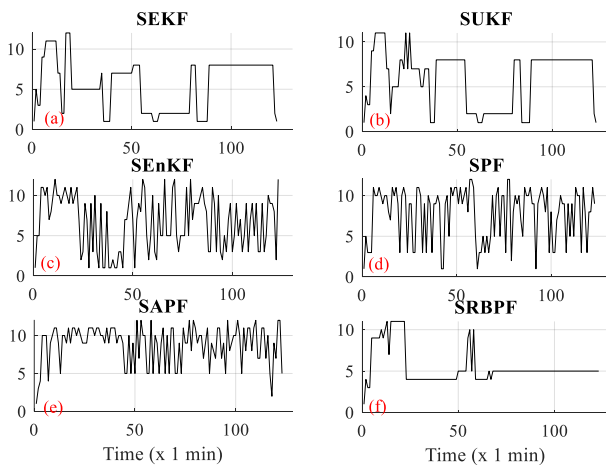
Figure 13. Switched model from M1 to M12 by (a) SEKF (b) SUKF (c) SEnKF (d) SPF (e) SAPF (f) SRBPF

Utilizing the information of switched models, the HI and RUL can be switched from 12 models for each estimator, which are performed in Figure 14 (a) and (b). The switched HI tracks well the real HI in Figure 14 (a). Before 80 (x 1 min), switching EKF and UKF show a relative smooth RUL, both curves deviate far from real RUL before 20 (x 1 min), then converge till 50 (x 1 min). After that, they start to have a decreasing life. Switching EnKF follows similar trend as SEKF and SUKF, but more closer to real RUL. However, switching PF presents more fluctuation due to the frequent switch, but estimates RUL more accurately before 40 (x 1 min). By comparison, the estimated RUL by switching APF has a similar behavior with SPF. After the 80 (x 1 min), the RUL by switching RBPF convenes together with other switching estimators, however, it possesses a larger error between 20 (x 1min) and 50 (x 1 min).
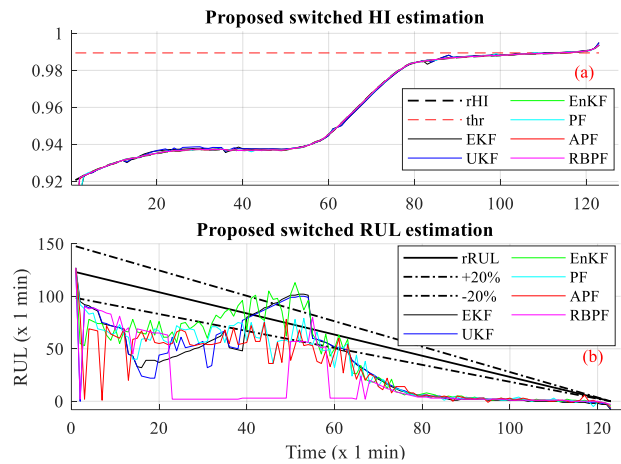
Figure 14. (a) Switched HI estimation (b) Switched RUL estimation of B11 by proposed approach

To better compare the seven estimators of Section 2.2 and the twelve models of Table 2, the Root Mean Squared Error (RMSE) between the real RUL and the estimated RUL for the whole time are compared in Figure 15 (a) and (b). In Figure 15 (a), 12 models and the proposed switched model 'sM' are compared for each estimator. In the cluster of bars of EKF, 'M9' and 'M1' have the least error. Excepting the large error of 'M4' and 'M6', the proposed mixture models ('M7',…,'M12') achieve equivalent or better performance than the classic exponential models. Analyzing other estimators, 'M9' and 'M1' win other models in most cases. It should be mentioned that the proposed 'sM' does not give the best RUL estimation, but surpasses many single models. In Figure 15 (b), the performance of estimators for each model is presented. For 'M1', PF achieves best RUL estimation, then APF and UKF follows. By contrast, EnKF surges the highest RMSE for 'M1', while RBPF and EKF reach a moderate performance. Checking all other models, EnKF shows less error for most of cases. In the view of model performance, 'M9' and 'M3' give out a relative smaller error than others.
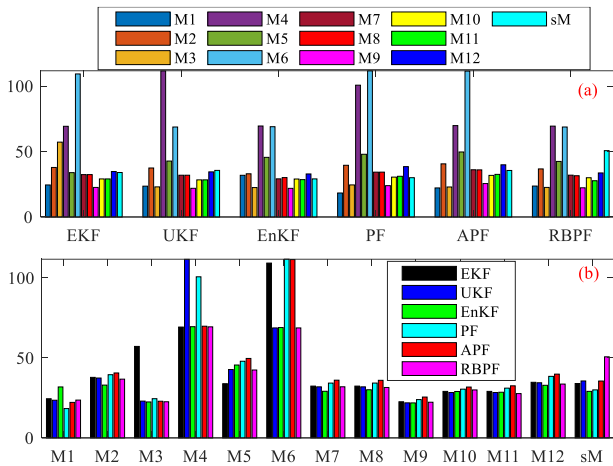
Figure 15. RMSE comparison in the cluster of (a) estimators (b) statistical models

In addition to the visual results for B11, comparisons of estimated RULs by the single models of Table 2 are summarized in Table 4. For each estimator, a value in format of 'X/Y' is given, where 'X' stands for the minimal RMSE of the 12 models, and 'Y' is the corresponding model index. For the bearing B11, although 'M9' has minimal error for most estimators, PF with 'M1' achieves the minimum error. Regarding the B12, 'M9' achieves still the least error in combination with UKF, EnKF and RBPF. However, the EKF with the 'M3' shows superior performance. Analyzing B13, 'M3' performs best with almost all estimators. Checking all other bearings, it can be found that the 'M9' and 'M3' appears most frequently over all estimators. M1' and 'M6' follow. In the aspect of an estimator with a single model, the EnKF achieves the best performance for the 15 bearings. Then, the APF and the UKF have a followed performance. Using the proposed MME strategy, the estimated RULs by switching MME and classic SKF are compared in Table 5. Switching RBPF and APF have won the most cases among the 15 bearings. It should be mentioned that the extended MME achieves better RUL than the classic SKF.

Table 4. RMSE comparison of estimators with single model

	EKF	UKF	EnKF	PF	APF	RBPF
B11	22.6/9	21.9/9	21.9/9	**18.3/1**	22.2/1	22.8/9
B12	**57.9/3**	69.3/9	68.3/9	71.0/8	61.1/10	68.2/9
B13	18.0/1	**17.6/3**	18.5/3	18.4/3	18.2/3	17.9/3
B14	62.3/5	31.9/5	68.6/4	18.8/12	**11.4/3**	32.4/5
B15	24.1/13	23.3/13	**17.0/12**	21.6/1	21.3/11	20.2/1
B21	154.2/2	153.6/2	**150.8/10**	152.9/12	152.8/12	151.8/2
B22	23.4/1	22.1/3	24.1/1	24.8/1	**12.7/1**	21.8/3
B23	**182.9/9**	228.5/3	185.5/9	186.5/9	186.8/9	228.7/3
B24	95.4/3	**20.9/6**	21.2/6	40.6/4	40.9/4	21.7/6
B25	122.1/7	122.5/8	**116.5/8**	151.7/3	134.4/7	132.8/7
B31	1.9e3/5	1.7e3/9	2.2e3/12	**0.8e3/2**	0.9e3/2	1.9e3/3
B32	1.1e3/7	1.0e3/8	**0.7e3/9**	0.8e3/9	0.8e3	0.9e3/4
B33	9e2/3	6e2/3	**5e2/3**	1.3e3/3	1.3e3/3	6e2/3
B34	851.7/4	663.9/3	**578.9/3**	834.8/9	744.8/9	663.9/3
B35	35.1/6	32.1/6	**31.9/6**	60.5/6	63.3/6	31.9/6

Table 5. RMSE comparison of proposed switching MME

	CKF	EKF	UKF	EnKF	PF	APF	RBPF
B11	4.1e3	34.0	35.6	**29.1**	30. 0	35.5	50.7
B12	4.3e3	80.4	76.3	79.5	78.2	70.5	**68.4**
B13	2.7e3	91.3	92.8	65.3	61.6	**45.9**	3.0e3
B14	3.6e3	**117.0**	126.3	665.5	1.8e3	891.1	168.2
B15	3.6e3	24.1	23.3	30.3	23.6	**22.4**	29.5
B21	4.3e3	167.2	**163.1**	700.9	177.9	667.9	347.1
B22	3.4e3	67.3	66.6	55.6	50.0	**44.3**	45.0
B23	3.9e3	469.5	1.9e3	452.2	298.7	**271.3**	925.7
B24	2.9e3	144.6	140.2	149.3	**124.6**	145.3	150.1
B25	3.7e3	296.1	161.0	383.1	775.1	164.9	**139.1**
B31	2.4e3	2.3e3	**2.2e3**	2.3e3	2.4e3	2.4e3	2.4e3
B32	2.5e3	1.9e3	1.5e3	1.7e3	**1.3e3**	1.6e3	2.2e3
B33	4.4e3	**2.3e3**	3.1e3	3.0e3	3.4e3	3.3e3	2.5e3
B34	3.3e3	3.1e3	3.2e3	**2.8e3**	3.4E3	3.4e3	2.9e3
B35	2.8e3	188.4	187.9	216.3	189.0	185.4	**183.4**

Table 6. 'Err' comparison corresponding to Table 4

	EKF	UKF	EnKF	PF	APF	RBPF
B11	0.7	0.7	0.6	**0.9**	0.9	0.7
B12	**0.2**	1.0	1.0	1.0	-0.7	1.0
B13	-0.4	**-0.1**	-0.5	-0.5	-0.5	-0.2
B14	-0.9	-1.0	1.0	-1.0	**1.0**	-1.0
B15	0.7	0.7	**0**	0.9	0	0.6
B21	-0.9	-0.9	**-0.5**	0.2	0.2	-0.9
B22	0.3	-0.1	0.1	1.0	**-0.4**	0.2
B23	**0.7**	1.0	8.1e-2	0.1	0.1	1.0
B24	-1.0	**0.9**	0.9	1.0	1.0	0.9
B25	0.4	0.4	**0.6**	1.0	0.8	0.3
B31	3.0e-2	-0.6	-1.0	**-0.5**	-0.8	-0.5
B32	-0.3	-0.3	**7.9e-2**	0.5	0.4	0.9
B33	-1.0	-0.9	**-0.9**	-1.0	-1.0	-0.9
B34	2.3e-2	0.7	**0.6**	1.0	1.0	0.7
B35	-0.3	0.6	**0.8**	-1.0	-1.0	0.6

In order to quantify the overestimation or the underestimation of the estimated RUL, the magnitude of error ('Er') (Botchkarev 2018), measuring the point distance between the real RUL (rRUL) and the predicted RUL (pRUL), is adopted.

$$Er(i) = aRUL(i) - pRUL(i) \qquad (1)$$

$$\Delta(i) = \begin{cases} 1, if\ Er(i) > 0 \\ -1, if\ Er(i) < 0 \\ 0, if\ Er(i) = 0 \end{cases} \qquad (2)$$

$$Err = \frac{\sum_{i=1}^{L} \Delta(i)}{L} \qquad (3)$$

The performance of 'Er' at time index i is given in equation (1). As shown in equation (2), if 'Er' is positive, Δ is equal to 1. On the contrary, Δ is -1 if the RUL is overestimated. In case the RUL is perfectly estimated, Δ equals 0. To evaluate the overall performance of overestimation or underestimation for the whole estimation period, the criterion is further formulated as equation (3). If the overestimation occurs for the whole time indexes ($i = 1, ..., L$), 'Err' is equal to -1. Yet, 'Err' is equal to 1 if the RUL of all time indexes are

underestimated. However, if the curve of the predicted RUL coincides with the actual RUL, 'Err' is equal to 0.

Table 7. 'Err' comparison of proposed switching MME

	CKF	EKF	UKF	EnKF	PF	APF	RBPF
B11	-0.5	0.7	0.7	**0.6**	0.8	0.8	0.98
B12	-0.6	0.9	0.9	0.9	0.9	0.96	**0.99**
B13	3.8e-2	-0.8	-0.7	-0.7	-0.8	**-0.8**	-0.9
B14	-0.6	-1.0	**-1.0**	-1.0	-1.0	-1.0	-1.0
B15	0	0.7	0.7	0.1	0.4	**0.2**	0.4
B21	-0.8	-0.4	**-0.2**	-0.8	-0.8	-0.6	0.3
B22	-0.3	-0.3	-0.03	0.09	-0.2	**-0.3**	0.3
B23	-0.6	0.2	-0.4	-0.3	-0.7	**-0.6**	-0.8
B24	0.1	-1.0	-1.0	-0.3	**-1.0**	-1.0	-0.3
B25	-0.3	0.8	1.0	0.8	1.0	0.9	**0.6**
B31	-0.8	-0.9	**-0.8**	-0.9	-0.9	-1.0	-1.0
B32	-0.8	-0.5	-0.4	-0.3	**-0.1**	0	-0.5
B33	-0.8	**-0.9**	-0.9	-0.8	-0.9	-0.9	-0.8
B34	-0.8	-0.9	-1.0	**-0.8**	-1.0	-1.0	-0.7
B35	0.3	-0.2	0.2	0.11	0.7	0.7	**0.7**

The 'Err' of equation (3), corresponding to the estimator and the model in Table 4 and 5, is compared respectively in Table 6 and 7. In Table 6, it can be seen that the 'Err' of B11 remains positive for all estimators and indicated models of the Table 4, which means that the overall RUL has not been overestimated for the whole estimation period. The high value (0.9) of PF and APF represents that most estimated RUL values are underestimated compared to the actual RUL. Analyzing all bearings of Table 6, a similar phenomenon appears for B12, B15, B22, B23, B25, B34 and B35, whereas the negative 'Err' of the other bearings signify that there are more overestimated than underestimated RULs. With respect to the proposed MME, the 'Err' of each bearing is compared in Table 7. It is clear to notice that the 'Err' of the CKF present negative value for almost each bearing. Thus, the estimated RULs by CKF deliver not only the large RMSE (as shown in Table 5), but also the issue of the overestimation (as Table 7). Yet, most algorithms of the B11, B12, B15, B25 and B35 present positive 'Err'. Besides, the 'Err', corresponding to the minimal RMSE in Table 4 and 5, is highlighted in Table 6 and 7. The 1 and -1 of 'Err' exhibits that the RUL is underestimated or overestimated for all time indexes, respectively. It should be also addressed that the 'Err' with 0 in Table 6 and 7 do not stand for the perfect RUL estimation, but the large estimation error. In such a situation, the minimal 'Err' is caused in the aggregation phase, when the positive errors and negative errors cancel each other (Botchkarev 2018). However, combined with RMSE (as shown in Table 4 and 5), the falsely high accuracy by 'Err' can be recognized. In the face of drawbacks of RMSE, which evaluates only the overall estimation error, ignores the issue of the overestimation or underestimation, the deployed 'Err' helps to characterize this phenomenon.

5. CONCLUSION

In this paper, z multi-model based prognostics methodology is proposed and investigated on fifteen bearings. Firstly, by comparing a library of HIs (statistical indicators, entropy indicators and sparsity indicators), the quasi-arithmetic means achieve better trendability and prognosability than classical HIs. Secondly, a library of statistical models, including the state of the art exponential models and also the proposed mixture type of polynomial model and exponential model, are systematically investigated on each estimator. Through the comparison, the mixture type models and the Ensemble Kalman Filter perform well for the single model strategy, thus they can be potentially used for bearings' prognostics in the future. Thirdly, considering the drawbacks of the classic Switching Kalman Filter, applied only using three constant state space models, several versions of multi-model estimation are proposed and merge a library of nonlinear statistical models together. Although the proposed Multi-Model based prognostics only provides an intermediate performance, having not surpassed the best RUL estimation provided by the single model estimation, obtained from a particular model of the library, it can be mentioned that the proposed multi-model strategy supplies a solution for the challenge of model selection.

REFERENCES

Antoni, Jerome. 2016. "The Infogram: Entropic Evidence of the Signature of Repetitive Transients." *Mechanical Systems and Signal Processing* 74:73–94. doi: 10.1016/J.YMSSP.2015.04.034.

Arulampalam, M. Sanjeev, Simon Maskell, Neil Gordon, and Tim Clapp. 2002. *A Tutorial on Particle Filters for Online Nonlinear/Non-Gaussian Bayesian Tracking*. Vol. 50.

Botchkarev, Alexei. 2018. "Performance Metrics (Error Measures) in Machine Learning Regression, Forecasting and Prognostics: Properties and Typology." *Interdisciplinary Journal of Information, Knowledge, and Management* 14:45–76. doi: 10.28945/4184.

Gray, Augustine H., and John D. Markel. 1974. "A Spectral-Flatness Measure for Studying the Autocorrelation Method of Linear Prediction of Speech Analysis." *IEEE Transactions on Acoustics, Speech, and Signal Processing* 22(3):207–17. doi: 10.1109/TASSP.1974.1162572.

Hou, Bingchang, Dong Wang, Tangbin Xia, Yi Wang, Yang Zhao, and Kwok-leung Tsui. 2021. "Investigations on Quasi-Arithmetic Means for Machine Condition

Monitoring." *Mechanical Systems and Signal Processing* 151(April):107451. doi: 10.1016/j.ymssp.2020.107451.

Jamie, Coble, Hines, J. Wesley. 2009. "Identifying Optimal Prognostic Parameters from Data: A Genetic Algorithms Approach." in *Annual Conference of the Prognostics and Health Management Society 2009*.

Jin, Xiaohang, Zijun Que, Yi Sun, Yuanjing Guo, and Wei Qiao. 2019. "A Data-Driven Approach for Bearing Fault Prognostics." *IEEE Transactions on Industry Applications* 55(4):3394–3401. doi: 10.1109/TIA.2019.2907666.

Lim, Chi Keong Reuben, and David Mba. 2015. "Switching Kalman Filter for Failure Prognostic." *Mechanical Systems and Signal Processing* 52–53:426–35. doi: 10.1016/J.YMSSP.2014.08.006.

Meng, Huixing, and Yan Fu Li. 2019. "A Review on Prognostics and Health Management (PHM) Methods of Lithium-Ion Batteries." *Renewable and Sustainable Energy Reviews* 116:109405.

Mustière, Frédéric, Miodrag Bolić, and Martin Bouchard. 2006. "Rao-Blackwellised Particle Filters: Examples of Applications." Pp. 1196–1200 in *Canadian Conference on Electrical and Computer Engineering*. Institute of Electrical and Electronics Engineers Inc.

Pan, Y. N., J. Chen, and X. L. Li. 2009. "Spectral Entropy: A Complementary Index for Rolling Element Bearing Performance Degradation Assessment." *Proceedings of the Institution of Mechanical Engineers, Part C: Journal of Mechanical Engineering Science* 223(5):1223–31. doi: 10.1243/09544062JMES1224.

Roth, Michael, Gustaf Hendeby, Carsten Fritsche, and Fredrik Gustafsson. 2017. "The Ensemble Kalman Filter: A Signal Processing Perspective." *Eurasip Journal on Advances in Signal Processing* 2017(1):1–16.

Saidi, Lotfi, Jaouher Ben Ali, Mohamed Benbouzid, and Eric Bechhoefer. 2018. "Wind Turbine Drivetrain Prognosis Approach Based on Kalman Smoother with Confidence Bounds." Pp. 1865–70 in *Proceedings of the IEEE International Conference on Industrial Technology*. Vols. 2018-February. Institute of Electrical and Electronics Engineers Inc.

Singleton, Rodney K., Elias G. Strangas, and Selin Aviyente. 2015. "Extended Kalman Filtering for Remaining-Useful-Life Estimation of Bearings." *IEEE Transactions on Industrial Electronics* 62(3):1781–90. doi: 10.1109/TIE.2014.2336616.

Wang, Biao, Yaguo Lei, Naipeng Li, and Ningbo Li. 2020. "A Hybrid Prognostics Approach for Estimating Remaining Useful Life of Rolling Element Bearings." *IEEE Transactions on Reliability* 69(1):401–12. doi: 10.1109/TR.2018.2882682.

Wang, Peng, Ruqiang Yan, and Robert X. Gao. 2018. "Multi-Mode Particle Filter for Bearing Remaining Life Prediction." in *ASME 2018 13th International Manufacturing Science and Engineering Conference, MSEC 2018*. Vol. 3. American Society of Mechanical Engineers (ASME).

BIOGRAPHIES

Junyu Qi received an M.S. degree in Mechatronics from Shanghai Maritime University, Shanghai, China, in 2012 and from Friedrich-Alexander-University Erlangen-Nuremberg, Germany, in 2016, respectively. He is currently a PhD student in the Department of Mechanical Engineering of KU Leuven, Belgium. His research interests focus on condition monitoring of rotating machinery and particularly in prognostics.

Alexandre Mauricio received his MSc. degree in Mechanical Engineering from the Faculty of Engineering of the University of Porto (FEUP) in 2017. He is currently a PhD student at the Department of Mechanical Engineering of KU Leuven, Belgium. His main research interests focus on the diagnostics of rotating machinery operating under time varying conditions.

Konstantinos Gryllias holds a 5 years engineering diploma degree and a PhD degree in Mechanical Engineering from National Technical University of Athens, Greece. Since October 2014 he holds an assistant professor position on vibro-acoustics of machines and transportation systems at the Department of Mechanical Engineering of KU Leuven, Belgium. He is also the manager of the University Core Lab Dynamics in Mechanical & Mechatronic Systems DMMS-M of Flanders Make, Belgium. His research interests lie in the fields of condition monitoring, signal processing, prognostics and health management of mech. &mechatronic systems.